

Article

Optimization of Binary Adsorption of Metronidazole and Sulfamethoxazole in Aqueous Solution Supported with DFT Calculations

Juan Carlos Serna-Carrizales ¹, Ana I. Zárate-Guzmán ^{1,*}, Angélica Aguilar-Aguilar ¹, Angélica Forgianny ², Esther Bailón-García ³, Elizabeth Flórez ², Cesar F. A. Gómez-Durán ¹ and Raúl Ocampo-Pérez ^{1,*}

- ¹ Centro de Investigación y Estudios de Posgrado, Facultad de Ciencias Químicas, Universidad Autónoma de San Luis Potosí, Av. Dr. Manuel Nava 6, San Luis Potosí 78210, Mexico
- ² Grupo de Investigación de Materiales con Impacto, Mat&mpac. Facultad de Ciencias Básicas, Universidad de Medellín, Medellín 050026, Colombia
- ³ Research Group in Carbon Materials, Inorganic Chemistry Department, Faculty of Sciences, University of Granada, Campus Fuente Nueva s/n, 18071 Granada, Spain
- * Correspondence: aizg_08@hotmail.com (A.I.Z.-G.); raul.ocampo@uaslp.mx (R.O.-P.)

Abstract: Sulfamethoxazole [SMX] and metronidazole [MNZ] are emergent pollutants commonly found in surface water and wastewater, which can cause public health and environmental issues even at trace levels. An efficient alternative for their removal is the application of adsorption technology. The present work evaluated single and binary adsorption processes using granular activated carbon (CAG F400) for SMX and MNZ in an aqueous solution. The binary adsorption process was studied using a Box–Behnken experimental design (RSD), and the results were statistically tested using an analysis of variance. Density functional theory (DFT) modeling was employed to characterize the interactions between the antibiotics and the CAG F400 surface. For the individual adsorption process, adsorption capacities (q_e) of 1.61 mmol g⁻¹ for SMX and 1.10 mmol g⁻¹ for MNZ were obtained. The adsorption isotherm model that best fit experimental data was the Radke–Prausnitz isotherm model. The adsorption mechanism occurs through electrostatic and π - π dispersive interactions. For the binary adsorption process, the total binary adsorption capacity achieved was 1.13 mmol g⁻¹, evidencing competitive adsorption. The significant factors that determine the removal of SMX and MNZ from a binary solution were the solution pH and the initial concentration of antibiotics. From DFT studies, it was found that SMX adsorption on CAG F400 was favored with adsorption energy (E_{ads}) of -10.36 kcal mol⁻¹. Finally, the binary adsorption results corroborated that the adsorption process was favorable for both molecules.

Keywords: binary adsorption; sulfamethoxazole; metronidazole; activated carbon; adsorption energy



Citation: Serna-Carrizales, J.C.; Zárate-Guzmán, A.I.; Aguilar-Aguilar, A.; Forgianny, A.; Bailón-García, E.; Flórez, E.; Gómez-Durán, C.F.A.; Ocampo-Pérez, R. Optimization of Binary Adsorption of Metronidazole and Sulfamethoxazole in Aqueous Solution Supported with DFT Calculations. *Processes* **2023**, *11*, 1009. <https://doi.org/10.3390/pr11041009>

Academic Editors: Jan Derco, Andreja Žgajnar Gotvajn and Angelika Kassai

Received: 28 February 2023

Revised: 22 March 2023

Accepted: 23 March 2023

Published: 27 March 2023



Copyright: © 2023 by the authors. Licensee MDPI, Basel, Switzerland. This article is an open access article distributed under the terms and conditions of the Creative Commons Attribution (CC BY) license (<https://creativecommons.org/licenses/by/4.0/>).

1. Introduction

Pharmaceutical compounds include a variety of organic compounds, referred to as emerging pollutants (EPs), which represent a potential risk to human health and the environment [1]. Among the most common drugs are antibiotics, which are a great environmental concern because most of these have low biodegradability in aerobic conditions [2]. Antibiotics are used in humans and animals, but the organisms cannot fully absorb them, and they are released into the environment in an active form [3]. Then, antibiotics can create an adverse effect on aquatic fauna through bioaccumulation, and consequently, enter the food chain and the human body again [3]. Thus, the ingestion of antibiotic residues can alter the human microbiome and promote emergence and selection for bacteria resistance in the body [4]. Currently, one of the main concerns about the presence of antibiotics is that wastewater treatment plants have low removal efficiencies for these compounds, which facilitates their accumulation in surface, groundwater bodies [5–7]. This situation

increases the possibility of creating a selection pressure on environmental microbiomes, which can lead to the generation of antibiotic resistance reservoirs in the environment [4]. In this sense, to avoid the presence of these compounds in the environment, the design of efficient treatment systems for drug elimination at the source (manufacturing industries and hospital facilities) is necessary [8,9].

Sulfonamides and nitroimidazoles belong to the group of drugs that are generating the greatest interest, since these drugs are among the antibiotics most widely used for the treatment of bacterial infections in humans and animals [10,11]. Nitroimidazoles, are characterized by high water solubility and low biodegradability, leading to their accumulation and persistence within ecosystems [2], while sulfonamides are less soluble in water and are highly resistant to degradation [2,12]. Recent studies have focused on the removal of these compounds through several technologies, such as adsorption, membrane separation, biological processes, electrochemical oxidation, and advanced oxidation processes (UV/H₂O₂, Fe²⁺/H₂O₂, O₃) [13–15].

Adsorption processes, considered a conventional technology, have been widely studied for the removal of pharmaceutical compounds due to their easy application, low cost, high efficiency, large-scale application, and above all, because they do not involve the generation of toxic by-products or intermediates [16,17]. This technology has been applied successfully to 30 different antibiotic compound elimination [3]. Several adsorbents have been used for the adsorption of SMX and MNZ, such as clays, metal-organic frameworks, and activated carbon materials (AC). The last one is the most useful due to its excellent physicochemical stability and high specific surface area (500–2000 m² g⁻¹) [18,19]. In this sense, Ariyanto et al. [19] studied the effect of pore structure and surface oxidation of a nanoporous carbon on the adsorption performance of MNZ, finding that the oxidized carbon material favored MNZ adsorption. In the case of SMX, Li et al. [3] have evaluated the adsorption of SMX on AC, finding a maximum adsorption capacity of 26.77 mg g⁻¹. In our research group, the single adsorption of MNZ and SMX on AC has been carried out, finding that the adsorption process is dominated by π - π dispersive interactions [2,20]. Hence, previous studies have focused on the elucidation of the type of adsorption in single systems [21,22]. However, few studies have been orientated on understanding the interactions involved during the adsorption process in multicomponent systems [23] or have reported the modeling and optimization of multicomponent adsorption systems [24–26].

In some cases, more than a single pharmaceutical compound is present in an aqueous sample, making it necessary to optimize the adsorption process to promote the removal of all compounds present in the sample [27]. Particularly, there are no studies reported until now for the combination of sulfonamides and nitroimidazoles. In this sense, the aim of this work is to evaluate the single and binary adsorption of metronidazole and sulfamethoxazole in an aqueous solution using a commercial activated carbon. The results have been statistically analyzed to determine the best conditions for maximizing the removal of both pharmaceuticals as a function of the solution pH, temperature, and initial concentrations of both pharmaceuticals. Additionally, the interactions between functionalities on carbon surfaces and pharmaceutical molecules have been elucidated through theoretical models. The density functional theory framework was used to determine the order of adsorption of SMX and NMZ on activated carbon.

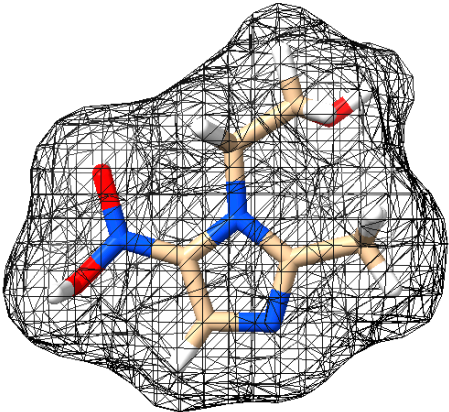
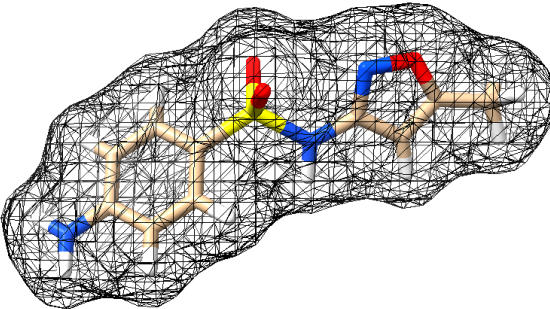
2. Materials and Methods

2.1. Materials

Sulfamethoxazole [SMX] and metronidazole [MNZ], supplied by Sigma Aldrich with 99% purity, were used as model pollutants. Table 1 shows the physicochemical properties of both molecules. The speciation diagrams (Figures 1 and 2) were constructed for both molecules considering the pK_a values. SMX is mostly present in its cationic form (SMX⁺) at pH < 3 due to the protonation of the amino group, while at pH values between 4 and 6.5, the molecule is neutral [SMX]. Finally, at pH > 8, the anionic form (SMX⁻) predominates

due to the deprotonation of the amino group. MNZ can also present in three forms when dissolved in water: at $\text{pH} < 4$, the protonated form of the molecule predominates (MNZ^+), at pH values in the range from 4 to 12, the molecule will be found mostly in its neutral form $[\text{MNZ}]$, while at $\text{pH} > 12$, the anionic form of the molecule (MNZ^-) will be predominant.

Table 1. Physicochemical properties of MNZ and SMX.

Physicochemical Property	MNZ	SMX
Structure		
Molecular formula	$\text{C}_6\text{H}_9\text{N}_3\text{O}_3$	$\text{C}_{10}\text{H}_{11}\text{N}_3\text{O}_3\text{S}$
Molecular weight (g mol^{-1})	171.15	253.28
pKa [28,29]	$\text{pK}_{\text{a}1} = 2.58$ $\text{pK}_{\text{a}2} = 14.44$	$\text{pK}_{\text{a}1} = 1.97$ $\text{pK}_{\text{a}2} = 6.16$
Solubility (mol L^{-1}) [28,29]	0.041	0.001109
Log Kow [30]	-0.02	0.9
Molecular size (nm)	$x = 0.969$ $y = 0.736$ $z = 0.454$	$x = 1.517$ $y = 0.676$ $z = 0.541$

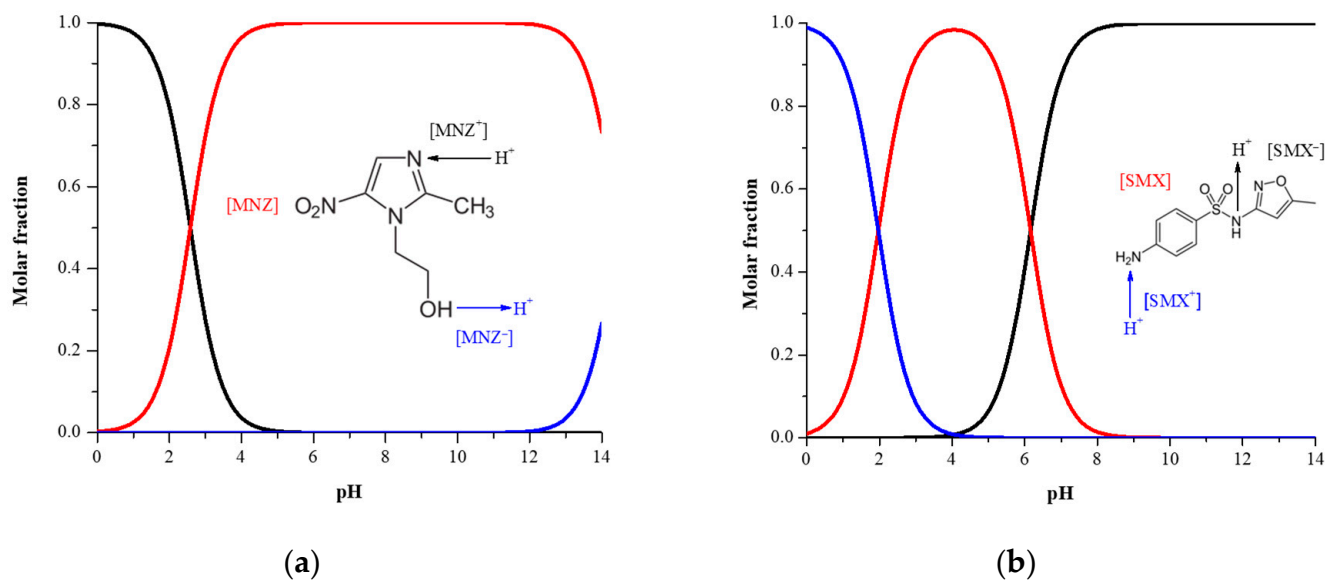


Figure 1. Speciation diagram of (a) MNZ and (b) SMX.

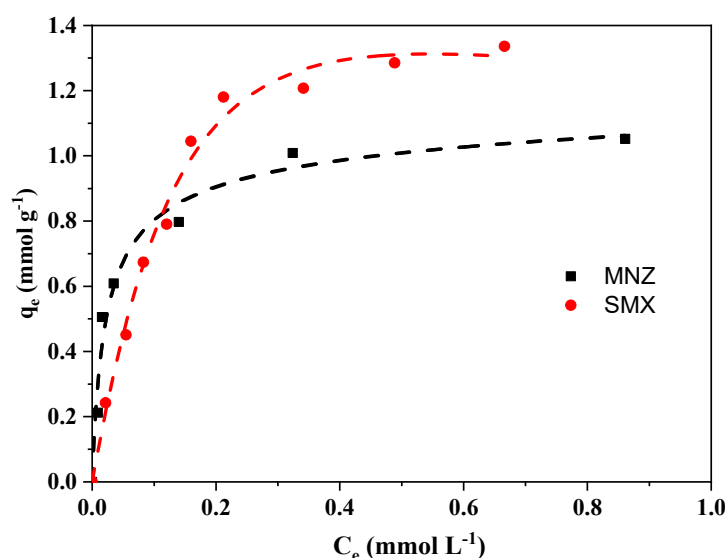


Figure 2. Individual adsorption isotherms of MNZ and SMX on GAC F400 at 25 °C and pH 7. The dotted line represents the prediction of the Radke–Prausnitz model.

2.2. Adsorbent

Filtrisorb 400 (F400) granular activated carbon (GAC F400), provided by Carbon Calgon Corporation, was used as an adsorbent. GAC F400 is made from select grades of bituminous coal through a process known as reagglomeration. The carbon was sieved to an average particle size of 0.541 mm. The chemical and textural properties of F400 GAC have been previously reported by Serna-Carrizales et al. [22]. The textural characterization of the GAC F400 is shown in Table S1 and Figure S1 of the supplementary material. The material presents a surface area (S_{BET}) of $756 \text{ m}^2 \text{ g}^{-1}$ and is mainly microporous. In terms of chemical properties, GAC F400 is characterized by a high concentration of total basic sites (0.486 meq g^{-1}) and a point of zero charge value ($\text{pH}_{\text{pzc}} = 9.43$) [22].

2.3. Concentration Determination of Sulfonamides and Nitroimidazoles

The concentration of sulfamethoxazole [SMX] and metronidazole [MNZ] in an aqueous solution were determined by high-performance liquid chromatography (HPLC) using Alliance e2695 equipment equipped with a diode array detector (wavelength 265 nm). The mobile phase consisted of a 0.1% acetic acid solution and acetonitrile in a 70/30 ratio, respectively, which were fed to the apparatus at a flow rate of 1 mL min^{-1} . The injection volume of both samples was $10 \text{ }\mu\text{L}$ and the retention time was 1.3 and 2.9 min for MNZ and SMX, respectively.

2.4. Obtaining Adsorption Equilibrium Data: Individual and Multicomponent

Experimental adsorption equilibrium data for both molecules were obtained using a batch adsorber. This system has been previously reported by Serna-Carrizales et al. [22] and consists of a set of vials of 50 mL capacity, which are immersed in a temperature-controlled bath. For the single adsorption process, the initial concentrations were set in a range from 0.02 to 2.3 mmol g^{-1} for MNZ, and from 0.089 to 1 mmol g^{-1} for SMX. For the binary adsorption process, the initial concentrations of both molecules were set in a range from 0.02 to 0.3 mmol L^{-1} , due to the solubility limitations of the SMX molecule. In all cases, 50 mL of a solution of known initial concentration was placed in the adsorbers, and a sample of 10 mL was taken from each vial to verify the initial concentration. Subsequently, 0.01 g of GAC F400 was added to each adsorber and immersed in a bath at a constant temperature until equilibrium was reached. During this period, the pH of the solution was kept constant by adding drops of NaOH or HCl as needed. After equilibrium was reached, a 1 mL aliquot was taken from each adsorber, and the concentration of the solute(s) present

was quantified. The individual adsorption capacity of the GAC F400 was obtained by the following mass balance:

$$q = \frac{V(C_{A0} - C_e)}{m} \quad (1)$$

where q is the amount of drug adsorbed (mmol g^{-1}); V is the volume of the solution (L); C_{A0} is the initial concentration of the solution (mmol L^{-1}); C_e is the equilibrium concentration (mmol L^{-1}); and m is the mass of GAC F400 employed (g).

The total adsorption capacity of GAC F400 for the binary system was calculated by summing the individual adsorption capacity according to the following relationship:

$$q_T = q_{MNZ} + q_{SMX} \quad (2)$$

To evaluate the effect of the system operating variables (pH, temperature, initial SMX concentration, and initial MNZ concentration), a Box–Behnken response surface design of experiments was used. Table S2 shows the experimental design used to obtain the binary equilibrium data, which consisted of four factors at three levels, each with three replicates of the central point, resulting in a total of 27 experiments. The minimum and maximum pH values were set in a range from 2 to 10, while the temperatures were set in a range from 10 to 40 °C. Finally, the experimental data were fitted to a second-order polynomial regression model, which is represented by the following general equation:

$$q = \beta_0 + \beta_1 \times pH + \beta_2 \times T + \beta_3 \times [MNZ] + \beta_4 \times [SMX] + \beta_5 \times pH \times T + \beta_6 \times pH \times [MNZ] + \beta_7 \times pH \times [SMX] + \beta_8 \times T \times [MNZ] + \beta_9 \times T \times [SMX] + \beta_{10} \times [MNZ] \times [SMX] + \beta_{11} \times pH^2 + \beta_{12} \times T^2 + \beta_{13} \times [MNZ]^2 + \beta_{14} \times [SMX]^2 \quad (3)$$

where β_0 is the independent term; β_{1-14} are the model coefficients; $[MNZ]$ and $[SMX]$ are the initial concentrations of metronidazole and sulfamethoxazole, respectively, (mmol L^{-1}); T is the temperature of the system (°C); and q represents the adsorption capacity of MNZ or SMX (mmol g^{-1}).

2.5. Characterization of the Antibiotic-Surface Interaction

The interactions between the antibiotics and the carbonaceous material were characterized through theoretical models. First-principles calculations were performed using the density functional theory framework (DFT). The calculations were performed with the Gaussian09 software using the DFT-B3LYP method and the 6-31+g(d,p) set of bases, which has been widely used for the study of these systems. The geometry optimization calculations were carried out considering the solvent effect, using the IEFPCM approximation (integral equation formalism variant of the polarized continuum model). The values of the local potential energy minima for each structure were confirmed by the non-occurrence of imaginary frequencies. The adsorption energy was calculated using the following expression:

$$E_{ads} = E_{(antibiotic+surface)} - E_{antibiotic} - E_{surface} \quad (4)$$

where E_{ads} represents the adsorption energy; $E_{antibiotic+surface}$ corresponds to the total energy of the antibiotic complex/carbonaceous surface; $E_{antibiotic}$ is the energy of the antibiotic; and $E_{surface}$ is the energy of the carbonaceous surface.

3. Results and Discussion

3.1. Single and Multicomponent Adsorption Equilibrium

3.1.1. Individual Adsorption Equilibrium

To perform a comparative analysis, the individual adsorption isotherms of MNZ and SMX were obtained (Figure 2). Both isotherms present an asymptotic “L” type behavior, which, according to Giles’ classification, indicates that the aromatic rings present in the structure of SMX and MNZ adsorb parallel to the graphitic planes of the GAC F400; this

behavior has been previously documented by Serna-Carrizales et al. [22] and Carrales-Alvarado et al. [20,31]. In Figure 2, it can be observed that at equilibrium concentrations (C_e) lower than 0.15 mmol L^{-1} , the carbon surface showed a slightly better affinity by MNZ, however, at higher concentrations at equilibrium, SMX adsorbed much better than MNZ. As an example, at an equilibrium concentration of 0.6 mmol L^{-1} , the adsorption capacity towards SMX and MNZ were 1.3 and 1.04 mmol g^{-1} , respectively.

This can be attributed to the isoxazole and aniline aromatic rings providing a high electron density in SMX; besides in SMX, more resonance structures can be proposed to stabilize this molecule. The two aromatic rings infer coplanarity, enhancing the π - π stacking interactions that it has with the GAC F400 surface. Moreover, at the experimental conditions ($\text{pH} = 7$ and $T = 25 \text{ }^\circ\text{C}$) the GAC F400 surface is positively charged. If we analyze the speciation diagram of both molecules (Figure 1), at a pH of 7, the SMX molecule is found mostly in its deprotonated form with the presence of neutral species, favoring adsorption through attractive electrostatic interactions and π - π interactions. In the case of the MNZ molecule, it is in its neutral form in a range of pH from 6 to 12. Thus, π - π interactions will be predominant in the adsorption process. However, MNZ has two disadvantages in the adsorption process. The first one is that, although MNZ possesses an imidazole ring, the electron density is diminished due to the nitro group, which is an electron-withdrawing group. This decreases the electronic density over the aromatic ring. The second disadvantage is the structure of MNZ; this molecule is only planar in the imidazole ring, therefore, the interaction area for π - π stacking interactions is smaller than SMX. The discussion about this behavior during adsorption will be supported by the computational results presented in Section 3.2, associated with the different established interactions between the antibiotics and the surface of GAC F400.

The experimental data were interpreted using the Langmuir, Freundlich, and Radke–Prausnitz isotherm models (see the supplementary material). The isotherm parameters were determined by the non-linear least-squares method using the Levenberg–Marquardt optimization algorithm and are shown in Table S3. The average deviation percentage (%D) was calculated to determine the best fit between the experimental data and the model (see supplementary material). Considering the values of the regression coefficient (R^2) and the average deviation percentage (%D) of each model, the Radke–Prausnitz and Langmuir isotherm models (Figure 2) describe the experimental data adequately. The maximum adsorption capacities from the Langmuir model were 1.61 mmol g^{-1} and 1.10 mmol g^{-1} for SMX and MNZ, respectively. These values are similar to those obtained in the literature using activated carbon [20,22].

3.1.2. Binary Adsorption Equilibrium

The binary adsorption process was analyzed through a response surface design of experiments. The experimental data were analyzed using Design-Expert 7.0 software. A significance level of 95% ($\alpha = 0.05$) was used to analyze the significance of the model and its respective coefficients. In this sense, the p -value is used to denote the significance of each factor as follows: the factor is statistically significant if the p -value is <0.05 , while a p -value > 0.05 lacks statistical significance. However, because some factors were around 5%, a refinement of the factors was performed by increasing the significance level to 90% ($\alpha = 0.1$) to cover all the factors that were affecting the system. Table S4 shows the analysis of variance (ANOVA) for the variable q_{SMX} . The statistically significant factors for this variable are the linear terms pH , T , and $[SMX]$, the interaction between the pH and $[SMX]$ and the quadratic terms pH^2 , T^2 , and $[SMX]^2$. From the values of F and p reported in Table S4, the $[SMX]$ term is the factor most influencing the q_{SMX} given that it shows the largest F value and the smallest p value. Finally, the model showed a p value < 0.0001 with no significant lack of fit, which indicates that the model can describe the change of q_{SMX} as a function of the factors studied.

The final model to describe the q_{SMX} , after a depuration process and considering the factors hierarchy, is represented by the following equation:

$$q_{SMX} = (0.0160 + 0.0576 \times pH - 8.955 \times 10^{-3} \times T + 5.278 \times [SMX] - 0.173 \times pH \times [SMX] - 4.340 \times 10^{-3} \times pH^2 + 1.920 \times 10^{-4} \times T^2 - 7.945 \times [SMX]^2)^2 \quad (5)$$

A similar analysis was performed to identify the significant terms during the adsorption of MNZ, q_{MNZ} , supported by the ANOVA analysis showed in Table S5. For this case, the statistically significant factors were the pH , $[SMX]$, $[MNZ]$, pH^2 , and the interaction between pH and $[MNZ]$. The mathematical model to describe the q_{MNZ} is given by the following equation:

$$q_{MNZ} = 0.0169 + 0.0613 \times pH + 0.830 \times [MNZ] - 0.374 \times [SMX] + 0.171 \times pH \times [MNZ] - 6.867 \times 10^{-3} \times pH^2 \quad (6)$$

Figure S2a,b shows the correlation between the experimental data for q_{SMX} and q_{MNZ} , respectively, and a random distribution can be observed over the 45° line for both cases when using Equations (5) and (6). Furthermore, the values of R^2 for the mathematical models were 0.9658 and 0.9426, respectively, which indicates that Equations (5) and (6) can predict the response successfully.

Finally, for the variable q_{TOTAL} (Table S6), the significant parameters are the linear terms pH , $[MNZ]$, and $[SMX]$, the interaction between pH and $[SMX]$, and the quadratic factors pH^2 and $[SMX]^2$. In this sense, the expression for q_{TOTAL} , considering the statistically significant terms, is described below:

$$q_{Total} = -0.541 + 0.214 \times pH + 1.661 \times [MNZ] + 5.411 \times [SMX] - 0.360 \times pH \times [SMX] - 0.0162 \times pH^2 - 8.220 \times [SMX]^2 \quad (7)$$

From the above equations, response surface curves were obtained for q_{MNZ} and q_{SMX} as a function of significant variables defined in Tables S4–S6. In Figure 3a, the variation of q_{MNZ} as a function of pH and $[SMX]$ at initial MNZ concentrations of 0.03, 0.16, and 0.30 mmol L⁻¹ is shown. The results reveal that q_{MNZ} is drastically dependent on the initial MNZ concentration, increasing favorably as the concentration of MNZ increases. As an example, at pH 6 and an initial SMX concentration of 0.2 mmol L⁻¹ the values of q_{MNZ} were 0.6, 0.4, and 0.2 mmol g⁻¹, at initial MNZ concentration of 0.30, 0.16 and 0.03 mmol L⁻¹, respectively. In Figure 3a, it can also be seen that pH has a significant influence on q_{MNZ} , but mainly at initial concentrations greater than 0.16, regardless of the presence of SMX.

Generally, it is observed that an increase in pH solution and initial MNZ concentration increases the adsorption capacity of MNZ. This effect is maximized at pH ≈ 8, which is associated with the fact that π-π stacking interactions are favored at this pH. Moreover, it can be observed that the presence of SMX during MNZ adsorption has a slight effect, i.e., the q_{MNZ} only decreases by 10% by increasing the initial SMX concentration from 0 to 0.3 mmol L⁻¹, indicating non-competitive adsorption during MNZ adsorption. At acidic pHs (≈pH 2), the adsorption capacity for MNZ presents the lowest values, since MNZ is mostly positively charged with a slight presence of a neutral charge, and GAC F400 is positively charged. This leads into the establishment of repulsive electrostatic interactions that decrease the adsorption capacity. In addition, MNZ in neutral form decreases significantly the electron density in the imidazole ring due to the nitro group disfavoring the π-π stacking interactions at this pH. Finally, during the adsorption of MNZ in the presence of SMX, the temperature was not a significant parameter. Carrales-Alvarado et al. [20] showed that during single adsorption of MNZ on activated carbon, the adsorption capacity at 10, 20, and 35 °C was not affected by temperature.

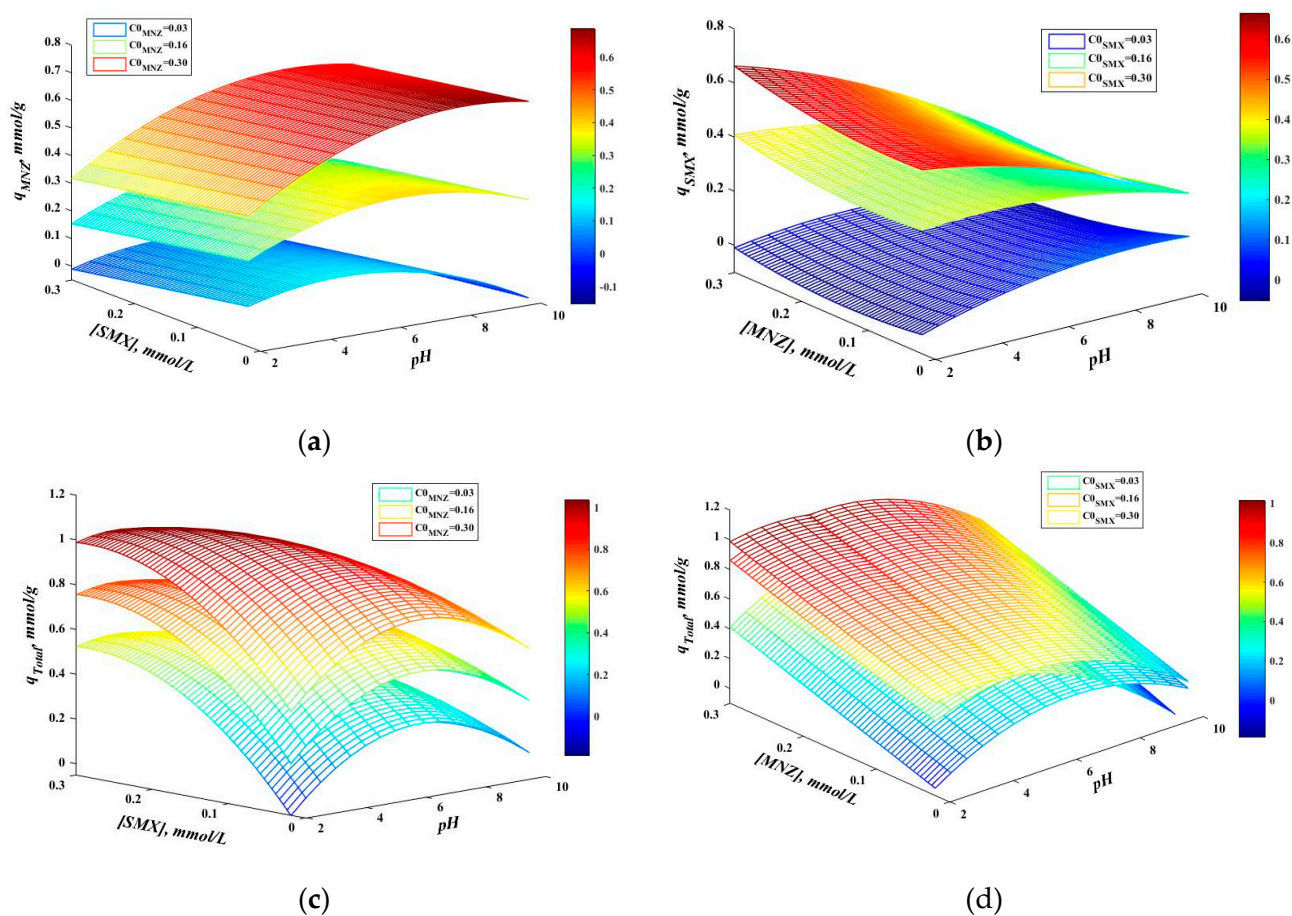


Figure 3. Surface response curves for (a) q_{MNZ} , (b) q_{SMX} , and (c) q_{TOTAL} in the function of $[SMX]$ and pH ; (d) q_{TOTAL} in the function of $[MNZ]$ and pH .

Figure 3b shows the variation of q_{SMX} as a function of $[MNZ]$ and the solution pH at different initial SMX concentrations. For an initial SMX concentration of 0.16 and 0.3 mmol L⁻¹, the adsorption capacity of SMX decreases by increasing the pH. This is congruent with the behavior found in the single system because, at pH values higher than 10, SMX is mostly negatively charged, as is the GAC F400 surface, causing repulsive electrostatic interactions. The highest adsorption capacity of SMX is found at low pH (pH = 2) regardless of the presence of MNX, where SMX is neutral and positive in a 1:1 ratio [2]. At this pH there is a protonated amido group that generates a positive charge in the molecule, but it seems that is not a positive charge strong enough to have significant repulsive interactions with GAC F400. Besides, the aniline and isoxazole rings possess high electron densities that favor the π - π stacking interactions [2]. In Figure 3b it can be seen that the presence of MNZ in the binary process does not affect the adsorption of SMX regardless of solution pH. However, at $[MNZ]$ concentrations of 0.16 and 0.30 mmol L⁻¹ at pH 2, the presence of MNZ significantly affects the adsorption capacity of SMX. As an example, at $[SMX]$ of 0.16 mmol L⁻¹ in the absence of MNZ, the adsorption capacity is $q_{SMX} = 0.2$ mmol g⁻¹, but in the presence of MNZ (0.3 mmol L⁻¹) the adsorption capacity is duplicated. Thus, SMX adsorption increased because the MNZ molecules provide order to adsorption process. We propose that MNZ is adsorbed between SMX molecules, and this action generates a stable adsorption process. Furthermore, π - π stacking interactions between SMX and MNZ contribute to a more stable stacking process. Since SMX and MNZ's electron densities in their aromatic rings are different, this generates stronger π - π interactions. MNZ rings are deactivated by the nitro group, and SMX is an amino group-activated ring. This difference in electron density favored stacking among different rings.

Figure 3c shows the behavior of total adsorption capacity concerning SMX concentration and pH. The total adsorption capacity increases with the rising solution concentration of both MNZ and SMX. This is consistent with the results shown in Table S2 since the highest q_{TOTAL} was found using the highest initial concentrations of SMX and MNZ (Exp 13). Additionally, comparing the maximum adsorption capacities found in individual systems ($q_{SMX} = 1.61 \text{ mmol g}^{-1}$ and $q_{MNZ} = 1.10 \text{ mmol g}^{-1}$) with the maximum total adsorption capacity found in the binary system ($q_{TOTAL} = 1.13 \text{ mmol g}^{-1}$), it is evident that the adsorption of SMX is affected by the presence of MNZ and vice versa in the binary system. This indicates that both molecules adsorb on the same active sites.

The effect of pH on q_{TOTAL} was also analyzed. It was found that at pH = 6, the q_{TOTAL} value is maximized. At this pH value, the MNZ molecule is entirely neutral, while the SMX molecule is 40% in its anionic form and 60% neutral, promoting π - π stacking interactions between the graphitic rings of GAC F400 and the aromatic rings of SMX and MNZ. Therefore, the best option is pH 6, since this will enhance the use of the active sites available in the GAC F400. According to these results, the mechanism that predominates during the binary adsorption of both antibiotics is governed by the occurrence of π - π stacking interactions, which are maximized at pH 6 with SMX concentrations higher than 0.15 mmol L^{-1} , and MNZ concentrations lower than 0.16 mmol L^{-1} . This can be seen in Table S6, from ANOVA, the interaction of $[SMX]$ and pH is significant because, in this pH range, the adsorption capacity of SMX is larger than that of MNZ.

The effect of $[MNZ]$ and pH over the total adsorption capacity is shown in Figure 3d. The values of q_{TOTAL} increase as the $[MNZ]$ and $[SMX]$ increase; this effect is observed at lower $[SMX]$ values (0.03 mmol L^{-1}). On the other hand, the pH value that maximizes the q_{TOTAL} was a value of 6. A similar behavior was found for SMX (see Figure 3c). Furthermore, the interaction between $[MNZ]$ and pH in the model design is not significant, therefore, pH does not affect the adsorption. Moreover, as is shown in Figure 1a, the speciation of MNZ does not change in a wide range of pHs.

3.2. Characterization of the Antibiotic-Surface Interaction

The possible interactions proposed between the surface functional groups present in the adsorbent and the antibiotics were modeled by computational calculations in monocomponent and multicomponent systems, according to the spectroscopic characterization of this material previously reported [32]. The carbonaceous surface was simulated, including functional groups, such as ether, semiquinone, carboxylic and phenol groups, with the last two of them being protonated species (that is, carboxylic H^+ [$-\text{COOH}_2^+$] and phenol H^+ [$-\text{OH}_2^+$]), considering that under experimental conditions at pH = 5, the surface is positively charged. A systematic study was carried out over these groups, considering the neutral and anionic forms of SMX molecules and the neutral form of MNZ (the neutral and anionic forms were established from speciation curves for both molecules). The adsorption energies (E_{ads}) for both contaminants are shown in Figure 4 (also see Table S7 in the supplementary material), and the stability of these geometries can be deduced based on the adsorption energies (see the most stable structures shown in Figure 5). In monocomponent systems, different interactions were established with the oxygenated groups of the carbonaceous material under four adsorption modes, i.e., interactions of a type where hydrogen bonds occur with ether, semiquinone, and the protonated carboxylic groups with the amine groups of SMX or MNZ molecules ($-\text{NH}$ or $-\text{NH}_2$) or with the $-\text{OH}$ group of MNZ. Also, π - π interactions and electrostatic attraction can take place between the functional groups and SMX (neutral and anionic forms) and MNZ molecules. Specifically, for SMX, aniline, isoxazole, and sulfonamide groups are determinants for interactions. For MNZ, the imidazole ring and nitro group are the principal sites for interactions. From these results, the stability sequence of the geometries obtained decreased in the following order for the proposed model with the SMX molecule: semiquinone > carboxylic H^+ > ether groups, while the order was semiquinone > ether > carboxylic H^+ groups was displayed with the MNZ molecule. Hence, these findings indicate that the affinity of the adsorption sites

for each pollutant depends on both; that is, the chemical nature of the adsorbent and the pollutant. In consequence, these results corroborated that the hydrogen bonds, electrostatic attraction, and π - π interaction mechanisms play an important role in the adsorption of the antibiotic molecules in these systems. From these results, it is possible also to propose that SMX adsorption is favored over the carbonaceous material compared to the MNZ molecule due to SMX's larger electron cloud created by the presence of aniline and isoxazole rings, which was evidenced by the experimental equilibrium results in monocomponent systems.

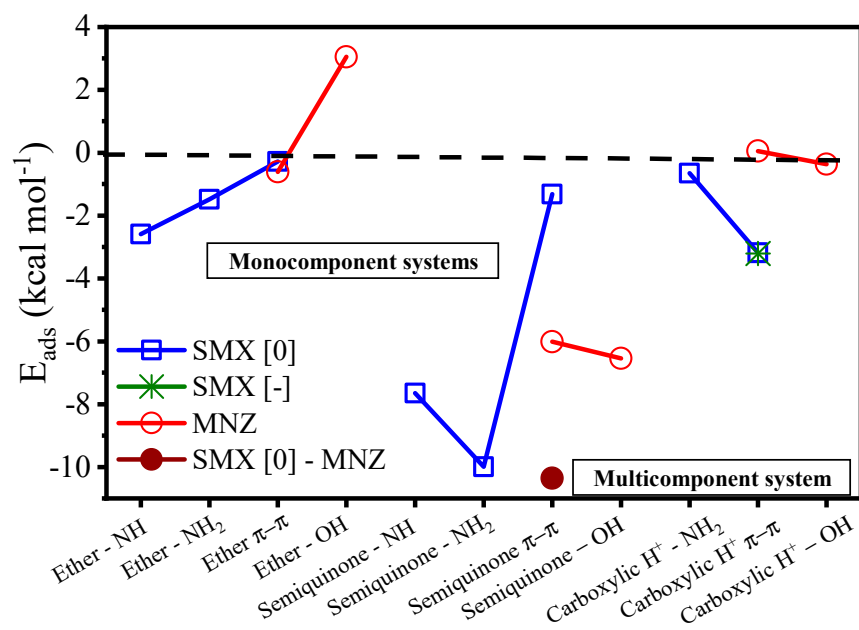


Figure 4. Adsorption energies (E_{ads}) for both antibiotics on functional groups of the models for the carbonaceous material in mono- and multicomponent systems.

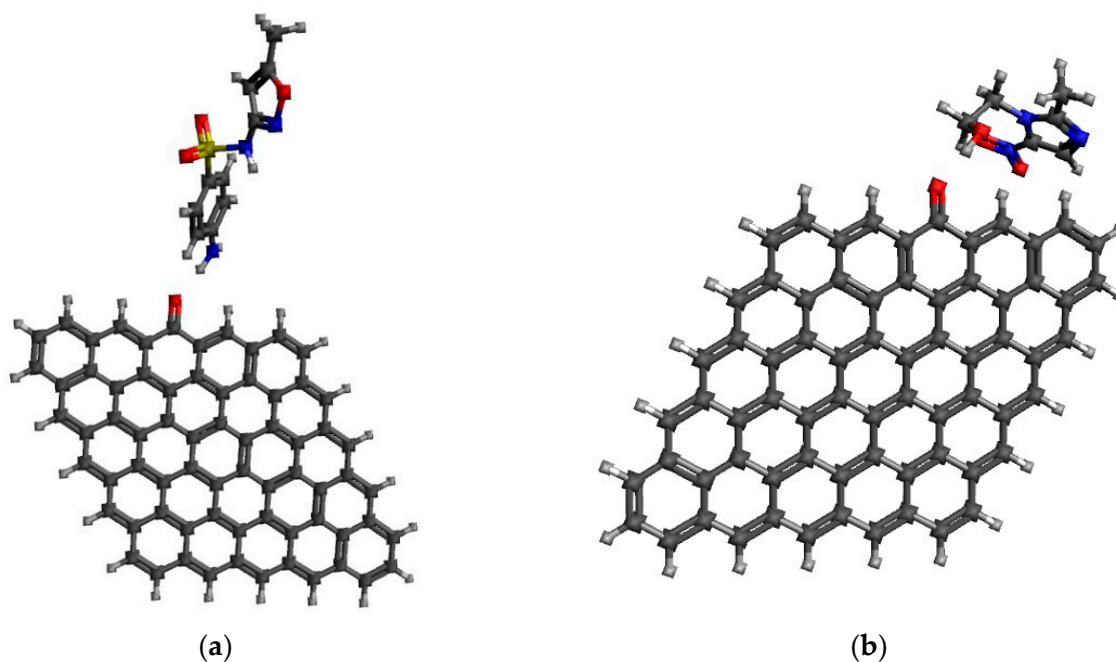


Figure 5. Cont.

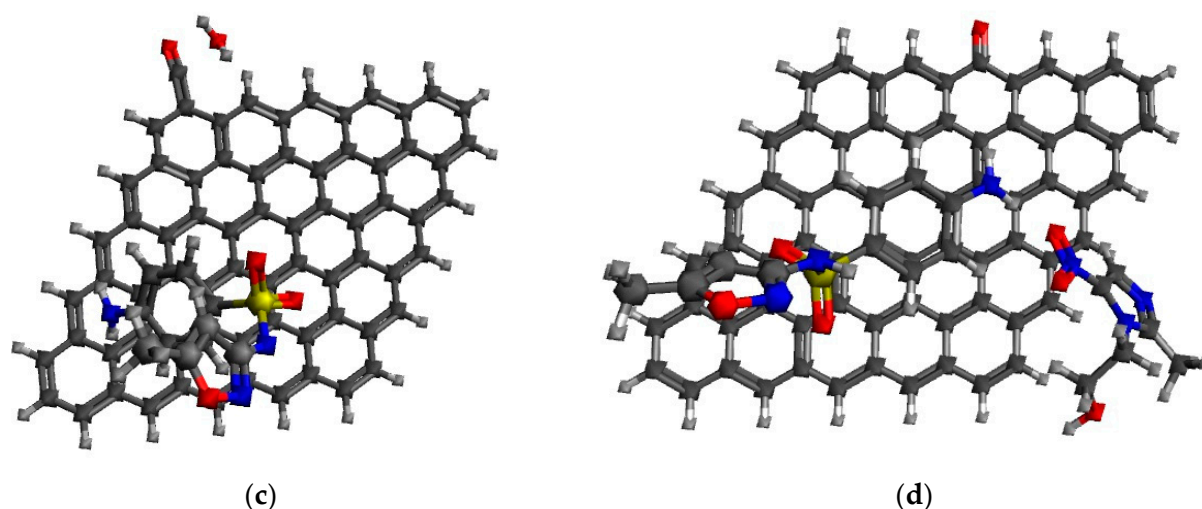


Figure 5. Most stable adsorption modes of antibiotic molecules on carbonaceous models. The C, O, H, N, and S atoms are symbolized by a dark gray, red, white, blue, and yellow color, respectively. (a) Semiquinone NH_2 -SMX [32], (b) Semiquinone OH-MNZ, (c) Carboxylic H^+ π - π -SMX [–], and (d) Semiquinone π - π -SMX [32]-MNZ.

For a multicomponent system, the adsorption of both antibiotics was evaluated over the carbonaceous surface containing the semiquinone group and considering π - π interactions among the surface and the antibiotic molecules (SMX and MNZ). The E_{ads} were favorable for the adsorption of both molecules with a value of $-10.36 \text{ kcal mol}^{-1}$, indicating that the SMX adsorption occurs first, followed by the MNZ, in a multicomponent system.

4. Conclusions

In the adsorption process, the concentration of the pharmaceutical compounds and the pH of the solution determined the affinity of GAC F400 towards SMX and MNZ molecules. Therefore, the best conditions to favor the adsorption process in a binary MNZ/SMX system are a pH of 6 and equimolar concentrations of each drug. The adsorption of SMX was affected by the presence of MNZ, so it can be inferred that there is a competitive adsorption process of an antagonistic type. For both drugs, the predominant adsorption mechanism is via electrostatic and π - π stacking interactions.

DFT models confirm the adsorption mechanism proposed. Also, the SMX adsorption is favored over the carbonaceous material compared to the MNZ molecule. In a binary system, SMX adsorption occurs first, followed by MNZ.

Supplementary Materials: The following supporting information can be downloaded at: <https://www.mdpi.com/article/10.3390/pr11041009/s1>.

Author Contributions: Conceptualization, J.C.S.-C., R.O.-P. and A.I.Z.-G.; methodology, J.C.S.-C. and A.I.Z.-G.; software, J.C.S.-C.; validation, R.O.-P., A.I.Z.-G., J.C.S.-C., A.F., E.B.-G., E.F., A.A.-A. and C.F.A.G.-D.; formal analysis, R.O.-P., A.I.Z.-G., A.F., E.F., A.A.-A. and C.F.A.G.-D.; investigation, J.C.S.-C., R.O.-P. and A.I.Z.-G.; data curation, J.C.S.-C., A.I.Z.-G., A.I.Z.-G. and A.F.; writing—original draft preparation, J.C.S.-C., R.O.-P., A.A.-A., A.F. and A.I.Z.-G.; writing—review and editing, J.C.S.-C., R.O.-P., A.F. and A.I.Z.-G.; visualization, J.C.S.-C., R.O.-P., A.I.Z.-G., A.F., E.F., A.A.-A. and C.F.A.G.-D.; supervision, R.O.-P. and A.I.Z.-G. All authors have read and agreed to the published version of the manuscript.

Funding: This research received no external funding.

Data Availability Statement: The data used to support the findings of this study are available from the corresponding author upon a reasonable request.

Acknowledgments: Juan Carlos Serna-Carrizales thanks the Consejo Nacional de Ciencia y Tecnología (National Council for Science and Technology), CONACyT, Mexico, for the funding granted for postgraduate studies. Dra. Ana I. Zárate-Guzmán thanks CONACyT for the support received through the “Convocatoria 2020: Estancias Posdoctorales por México” and “Convocatoria 2021: Segundo año de continuidad de Estancias Posdoctorales por México modalidades 1 y 2”.

Conflicts of Interest: The authors declare no conflict of interest.

References

1. Gondi, R.; Kavitha, S.; Yukesh Kannah, R.; Parthiba Karthikeyan, O.; Kumar, G.; Kumar Tyagi, V.; Rajesh Banu, J. Algal-Based System for Removal of Emerging Pollutants from Wastewater: A Review. *Bioresour. Technol.* **2022**, *344*, 126245. [[CrossRef](#)] [[PubMed](#)]
2. Moral-Rodríguez, A.I.; Leyva-Ramos, R.; Ocampo-Pérez, R.; Mendoza-Barron, J.; Serratos-Alvarez, I.N.; Salazar-Rabago, J.J. Removal of Ronidazole and Sulfamethoxazole from Water Solutions by Adsorption on Granular Activated Carbon: Equilibrium and Intraparticle Diffusion Mechanisms. *Adsorption* **2016**, *22*, 89–103. [[CrossRef](#)]
3. Li, R.; Sun, W.; Xia, L.; Zia, U.; Sun, X.; Wang, Z.; Wang, Y.; Deng, X. Adsorption of Toxic Tetracycline, Thiamphenicol and Sulfamethoxazole by a Granular Activated Carbon (GAC) under Different Conditions. *Molecules* **2022**, *27*, 7980. [[CrossRef](#)] [[PubMed](#)]
4. Ben, Y.; Fu, C.; Hu, M.; Liu, L.; Wong, M.H.; Zheng, C. Human Health Risk Assessment of Antibiotic Resistance Associated with Antibiotic Residues in the Environment: A Review. *Environ. Res.* **2019**, *169*, 483–493. [[CrossRef](#)] [[PubMed](#)]
5. Blair, B.D.; Crago, J.P.; Hedman, C.J.; Treguer, R.J.F.; Magruder, C.; Royer, L.S.; Klaper, R.D. Evaluation of a Model for the Removal of Pharmaceuticals, Personal Care Products, and Hormones from Wastewater. *Sci. Total Environ.* **2013**, *444*, 515–521. [[CrossRef](#)]
6. White, J.R.; Belmont, M.A.; Metcalfe, C.D. Pharmaceutical Compounds in Wastewater: Wetland Treatment as a Potential Solution. *Sci. World J.* **2006**, *6*, 1731–1736. [[CrossRef](#)]
7. Bilal, M.; Rizwan, K.; Adeel, M.; Iqbal, H.M.N. Hydrogen-Based Catalyst-Assisted Advanced Oxidation Processes to Mitigate Emerging Pharmaceutical Contaminants. *Int. J. Hydrogen Energy* **2022**, *47*, 19555–19569. [[CrossRef](#)]
8. Arzate, S.; Pfister, S.; Oberschelp, C.; Sánchez-Pérez, J.A. Environmental Impacts of an Advanced Oxidation Process as Tertiary Treatment in a Wastewater Treatment Plant. *Sci. Total Environ.* **2019**, *694*, 133572. [[CrossRef](#)]
9. Ghahari, S.; Ghahari, S.; Ghahari, S.; Nematzadeh, G.; Sarma, H. Integrated Remediation Approaches for Selected Pharmaceutical and Personal Care Products in Urban Soils for a Sustainable Future. *Energy Ecol. Environ.* **2021**, *7*, 439–452. [[CrossRef](#)]
10. Carvalho, I.T.; Santos, L. Antibiotics in the Aquatic Environments: A Review of the European Scenario. *Environ. Int.* **2016**, *94*, 736–757. [[CrossRef](#)]
11. Sarker, M.; Shin, S.; Jhung, S.H. Adsorptive Removal of Nitroimidazole Antibiotics from Water Using Porous Carbons Derived from Melamine-Loaded MAF-6. *J. Hazard. Mater.* **2019**, *378*, 120761. [[CrossRef](#)] [[PubMed](#)]
12. Guo, R.; Wang, Y.; Li, J.; Cheng, X.; Dionysiou, D.D. Sulfamethoxazole Degradation by Visible Light Assisted Peroxymonosulfate Process Based on Nanohybrid Manganese Dioxide Incorporating Ferric Oxide. *Appl. Catal. B* **2020**, *278*, 119297. [[CrossRef](#)]
13. Manjunath, S.V.; Singh Baghel, R.; Kumar, M. Antagonistic and Synergistic Analysis of Antibiotic Adsorption on Prosopis Juliflora Activated Carbon in Multicomponent Systems. *Chem. Eng. J.* **2020**, *381*, 122713. [[CrossRef](#)]
14. Prasannamedha, G.; Kumar, P.S. A Review on Contamination and Removal of Sulfamethoxazole from Aqueous Solution Using Cleaner Techniques: Present and Future Perspective. *J. Clean. Prod.* **2020**, *250*, 119553. [[CrossRef](#)]
15. Phoon, B.L.; Ong, C.C.; Mohamed Saheed, M.S.; Show, P.L.; Chang, J.S.; Ling, T.C.; Lam, S.S.; Juan, J.C. Conventional and Emerging Technologies for Removal of Antibiotics from Wastewater. *J. Hazard. Mater.* **2020**, *400*, 122961. [[CrossRef](#)]
16. Kumar, A.; Kumar, A.; Sharma, G.; Al-Muhtaseb, A.H.; Naushad, M.; Ghfar, A.A.; Stadler, F.J. Quaternary Magnetic BiOCl/g-C₃N₄/Cu₂O/Fe₃O₄ Nano-Junction for Visible Light and Solar Powered Degradation of Sulfamethoxazole from Aqueous Environment. *Chem. Eng. J.* **2018**, *334*, 462–478. [[CrossRef](#)]
17. Senthamarai, C.; Senthil-Kumar, P.; Priyadharshini, M.; Vijayalakshmi, P.; Vinoth, K.; Baskaralingam, P.; Thiruvengargaravi, K.V.; Sivanesan, S. Adsorption Behaviour of Methylene Blue Dye onto Surface Modified Strychnos Potatorum Seeds. *Environ. Prog. Sustain. Energy* **2012**, *33*, 676–680. [[CrossRef](#)]
18. Ahmed, I.; Adhikary, K.K.; Kim, K.; Ahn, W.S. Aqueous Adsorption of Sulfamethoxazole on an N-Doped Zeolite Beta-Templated Carbon. *J. Colloid Interface Sci.* **2021**, *582*, 467–477. [[CrossRef](#)]
19. Ariyanto, T.; Sarwendah, R.A.G.; Amimmal, Y.M.N.; Laksmiana, W.T.; Prasetyo, I. Modifying Nanoporous Carbon through Hydrogen Peroxide Oxidation for Removal of Metronidazole Antibiotics from Simulated Wastewater. *Processes* **2019**, *7*, 835. [[CrossRef](#)]
20. Carrales-Alvarado, D.H.; Leyva-Ramos, R.; Martínez-Costa, J.I.; Ocampo-Pérez, R. Competitive Adsorption of Dimetridazole and Metronidazole Antibiotics on Carbon Materials from Aqueous Solution. *Water Air Soil Pollut.* **2018**, *229*, 108. [[CrossRef](#)]
21. Pauletto, P.S.; Moreno-Pérez, J.; Hernández-Hernández, L.E.; Bonilla-Petriciolet, A.; Dotto, G.L.; Salau, N.P.G. Novel Biochar and Hydrochar for the Adsorption of 2-Nitrophenol from Aqueous Solutions: An Approach Using the PVSDM Model. *Chemosphere* **2021**, *269*, 128748. [[CrossRef](#)]

22. Serna-Carrizales, J.C.; Collins-Martínez, V.H.; Flórez, E.; Gomez-Duran, C.F.A.; Palestino, G.; Ocampo-Pérez, R. Adsorption of Sulfamethoxazole, Sulfadiazine and Sulfametazine in Single and Ternary Systems on Activated Carbon. Experimental and DFT Computations. *J. Mol. Liq.* **2021**, *324*, 114740. [[CrossRef](#)]
23. Forgiionny, A.; Acelas, N.Y.; Ocampo-Pérez, R.; Padilla-Ortega, E.; Pérez, S.; Flórez, E. Mechanism Adsorption Analysis during the Removal of Cd²⁺ and Cu²⁺ onto Cedar Sawdust via Experiment Coupled with Theoretical Calculation: Mono- and Multicomponent Systems. *Environ. Nanotechnol. Monit. Manag.* **2022**, *18*, 100715. [[CrossRef](#)]
24. Kavand, M.; Eslami, P.; Razeh, L. The Adsorption of Cadmium and Lead Ions from the Synthesis Wastewater with the Activated Carbon: Optimization of the Single and Binary Systems. *J. Water Process Eng.* **2020**, *34*, 101151. [[CrossRef](#)]
25. Gopinath, A.; Retnam, B.G.; Muthukkumaran, A.; Aravamudan, K. Swift, Versatile and a Rigorous Kinetic Model Based Artificial Neural Network Surrogate for Single and Multicomponent Batch Adsorption Processes. *J. Mol. Liq.* **2020**, *297*, 111888. [[CrossRef](#)]
26. Pauletto, P.S.; Lütke, S.F.; Dotto, G.L.; Salau, N.P.G. Forecasting the Multicomponent Adsorption of Nimesulide and Paracetamol through Artificial Neural Network. *Chem. Eng. J.* **2021**, *412*, 127527. [[CrossRef](#)]
27. Bagtash, M.; Zolgharnein, J. Crossed Mixture-Process Design for Optimization of Simultaneous Adsorption of Tartrazine and Indigo Carmine Dyes by Cobalt Hydroxide Nanosorbent. *J. Chemom.* **2018**, *32*, e3039. [[CrossRef](#)]
28. Asgari, E.; Sheikhmohammadi, A.; Yeganeh, J. Application of the Fe₃O₄-Chitosan Nano-Adsorbent for the Adsorption of Metronidazole from Wastewater: Optimization, Kinetic, Thermodynamic and Equilibrium Studies. *Int. J. Biol. Macromol.* **2020**, *164*, 694–706. [[CrossRef](#)]
29. Sun, Y.; Bian, J.; Zhu, Q. Sulfamethoxazole Removal of Adsorption by Carbon—Doped Boron Nitride in Water. *J. Mol. Liq.* **2021**, *349*, 118216. [[CrossRef](#)]
30. Mathon, B.; Coquery, M.; Liu, Z.; Penru, Y.; Guillon, A.; Esperanza, M.; Miège, C.; Choubert, J.M. Ozonation of 47 Organic Micropollutants in Secondary Treated Municipal Effluents: Direct and Indirect Kinetic Reaction Rates and Modelling. *Chemosphere* **2021**, *262*, 127969. [[CrossRef](#)]
31. Carrales-Alvarado, D.H.; Ocampo-Pérez, R.; Leyva-Ramos, R.; Rivera-Utrilla, J. Removal of the Antibiotic Metronidazole by Adsorption on Various Carbon Materials from Aqueous Phase. *J. Colloid Interface Sci.* **2014**, *436*, 276–285. [[CrossRef](#)] [[PubMed](#)]
32. Hernández-Padilla, E.S.; Zárate-Guzmán, A.I.; González-Ortega, O.; Padilla-Ortega, E.; Gómez-Durán, A.; Delgado-Sánchez, P.; Aguilar-Aguilar, A.; Cortés, F.B.; Ocampo-Pérez, R. Elucidation of Adsorption Mechanisms and Mass Transfer Controlling Resistances during Single and Binary Adsorption of Caffeic and Chlorogenic Acids. *Environ. Sci. Pollut. Res.* **2022**, *29*, 26297–26311. [[CrossRef](#)] [[PubMed](#)]

Disclaimer/Publisher’s Note: The statements, opinions and data contained in all publications are solely those of the individual author(s) and contributor(s) and not of MDPI and/or the editor(s). MDPI and/or the editor(s) disclaim responsibility for any injury to people or property resulting from any ideas, methods, instructions or products referred to in the content.